minerals

MDPI

Article

The Application of Integrated Geochemical and Geophysical Exploration for Prospecting Potential Prediction of Copper and Gold Polymetallic Deposits in the Fudiyingzi–Bacheli Area, Heilongjiang Province

Liang Chen [1,2], Huiyan Wang [3,*], Chengye Sun [4,*], Xiaopeng Chang [1,2] and Weizhong Ding [4]

[1] Center for Geophysical Survey, China Geological Survey, Langfang 065000, China; wansqsan@163.com (L.C.); changxpeng312@163.com (X.C.)
[2] Technology Innovation Center for Earth Near Surface Detection, China Geological Survey, Langfang 065000, China
[3] Research Center of Applied Geology of China Geological Survey, Chengdu 610039, China
[4] Institute of Geophysical and Geochemical Exploration, Chinese Academy of Geological Science, Langfang 065000, China; dk178@163.com
* Correspondence: wanghuiyan@mail.cgs.gov.cn (H.W.); schengye@mail.cgs.gov.cn (C.S.)

Abstract: The Duobaoshan mineralization area in Heilongjiang Province is a key copper–molybdenum–gold polymetallic region in China. Its southeastern Fudiyingzi–Bacheli area, located at the intersection of the NW-trending copper and NE-trending gold belts, exhibits favorable mineralization conditions. Despite over 70 years of placer gold mining and the discovery of one small copper deposit and one gold deposit, the area remains underexplored with significant peripheral exploration potential. This study integrates 1:50,000 geological mapping, high-precision magnetic surveys, phase-induced polarization, and soil geochemistry through multi-source data fusion for comprehensive mineral prediction. Key steps include delineating Cu, Au, and Mo anomalies and analyzing their associations with Zn, Cd, Ag, As, etc.; inferring NE-, NW-, and near-EW-trending linear structures via magnetic boundary enhancement; dividing high/low resistivity zones and identifying nine significant and six weak phase anomalies using phase-induced polarization; establishing a mineralization model based on typical deposits; and delineating four priority exploration targets. These results provide a scientific basis for further exploration in shallow coverage areas.

Keywords: Duobaoshan area; prospecting potential area; soil geochemistry; phase-induced polarization; magnetometry

check for updates

Academic Editors: Luigi Jovane and Saulo Pomponet Oliveira

Received: 19 March 2025
Revised: 27 May 2025
Accepted: 29 May 2025
Published: 2 June 2025

Citation: Chen, L.; Wang, H.; Sun, C.; Chang, X.; Ding, W. The Application of Integrated Geochemical and Geophysical Exploration for Prospecting Potential Prediction of Copper and Gold Polymetallic Deposits in the Fudiyingzi–Bacheli Area, Heilongjiang Province. *Minerals* **2025**, *15*, 597. https://doi.org/10.3390/min15060597

Copyright: © 2025 by the authors. Licensee MDPI, Basel, Switzerland. This article is an open access article distributed under the terms and conditions of the Creative Commons Attribution (CC BY) license (https://creativecommons.org/licenses/by/4.0/).

1. Introduction

The Duobaoshan area in Heilongjiang Province is a key copper–molybdenum–gold mineralization zone in China [1–4], with over 5.6 million tons of proven copper, 160,000 tons of molybdenum, and 130 tons of gold [5]. Its mineralization is controlled by the tectonic overlap of the Paleo-Asian Ocean and Pacific Plate [3,6,7]. Recent deep geophysical surveys reveal a conductive zone in the upper crust at the intersection of the NW-trending copper belt and NE-trending gold belt, suggesting deep material differentiation and the potential for large or super-large gold deposits. The Fudiyingzi copper mine and Bacheli gold–molybdenum mine have been identified in the Fudiyingzi–Bacheli region [8,9], but the systematic exploration of the surrounding 340 km² remains insufficient, hindering studies of mineralization patterns and exploration breakthroughs. At present, the formation

model of the Baicheli Gold Mine is still unclear. In contrast, the Fudigengzi Copper Mine is regarded as a typical volcanogenic massive sulfide (VMS)-type copper deposit, belonging to a type of marine multi-metal deposit. VMS-type copper deposits are widely distributed globally and have considerable resource reserves and good exploration prospects. According to statistics, the total number of known VMS deposits worldwide exceeds 800 [10]. The Fudigengzi Copper Mine is the only VMS-type deposit discovered in this region at present. An in-depth study of the mineralization characteristics and geological background of the Baicheli Gold Mine and the Fudigengzi Copper Mine will help promote new exploration breakthroughs in this region. In mineral prediction, three methods are commonly used: geological body (based on the ore-bearing rock distribution), single information (using mineralization points, alteration zones, and geophysical/geochemical anomalies), and comprehensive information (integrating the various anomalies, mineralization features, and rock distribution) [11]. Compared to the first two, the comprehensive method avoids single-method biases and offers greater advantages for concealed deposit prediction [12].

This study integrates 1:50,000 soil geochemistry, phase-induced polarization, and high-precision magnetic data to construct a "geology–geophysics–geochemistry–GIS" collaborative model. By analyzing typical deposits' ore-forming elements, a comprehensive mineral exploration model is established. The distribution of Cu, Au, and associated element anomalies is delineated, and NE-, NW-, and near-EW-trending structures are identified using magnetic boundary enhancement technology, addressing the deficiencies in fault identification in covered areas. Combined with phase-induced polarization-resistivity modeling, this approach enables the effective extraction of deep mineralization information and the prediction of prospective areas, providing a scientific basis for peripheral exploration in the Duobaoshan mineralized zone.

2. Metallogenic Background and Geology of the Study Area

2.1. Regional Metallogenic Background

The study area is located near the suture zone between the Xing'an and Songnen blocks in the eastern Central Asian Orogenic Belt, with the Duobaoshan island arc to the north [4,13–15]. Its geographical range is approximately 126°30′ E–127°00′ E and 49°30′ N–50°00′ N (Figure 1). This region experienced tectonic evolution involving the Paleozoic closure of the Paleo-Asian Ocean and Mesozoic Pacific Plate subduction. Active magmatic-tectonic activities provided the driving force and material sources for mineralization, forming two major systems [2,3,16]: (1) the NW-trending porphyry–skarn copper–molybdenum (gold) belt, including Sanmengou skarn-type iron–copper, Duobaoshan, and Tongshan porphyry-type copper–molybdenum deposits, related to Early Ordovician, Middle–Late Triassic, and Early–Middle Jurassic (partly Late Jurassic) magmatism [4,13–15,17]; and (2) the NE-trending gold belt, with Jurassic–Cretaceous mineralization (ca. 120–90 Ma), featuring skarn-type and epithermal gold deposits such as Sanmengou, Sandaowanzi, and Xiaoniuoheshui, influenced by Paleo-Pacific plate subduction [4,18]. The study area lies southeast of the intersection of these belts, where Fudiyingzi exhalative sedimentary Cu–Zn–Au and Bacheli Au–Mo deposits have been identified, showing multi-stage mineralization characteristics.

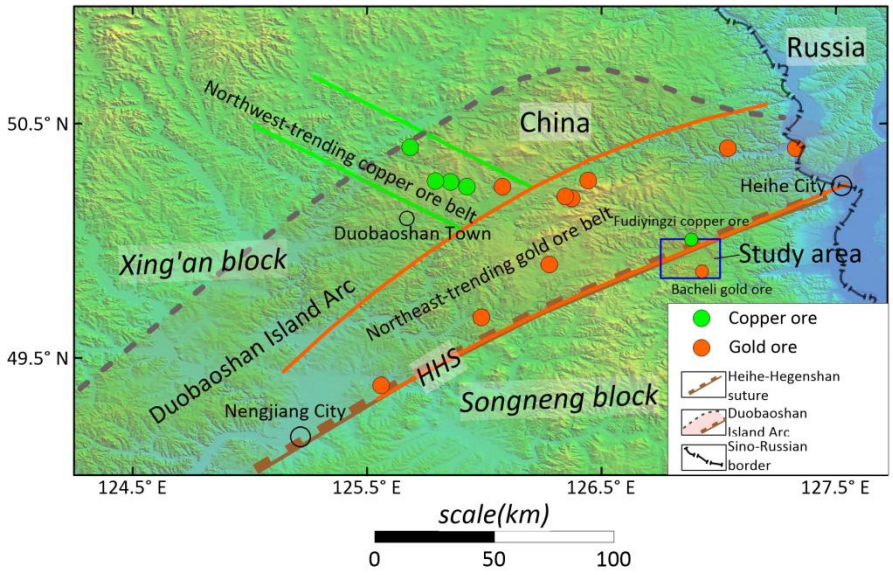


Figure 1. Regional tectonic map of the study area [13].

2.2. Geology of the Study Area

The stratigraphic sequence from oldest to youngest includes the following:

- Honghu Tuhe Formation (C_1hn): grayish-brown fine-grained tuff interbedded with rhyolitic crystal-lithic tuff and spotted slate, with local conglomerate layers;
- Dashizhai Formation (P_1d): greenish altered andesitic tuff breccia and altered basalt, hosting the Fudiyangzi copper deposit;
- Wudaoling Formation (P_2w): tuffaceous lava and grayish-black tuffaceous slate with pyritization;
- Ganhe Formation (K_1gn): consisting of basalt, andesitic basalt, and volcanic breccia;
- Guanghua Formation (K_1g): purple-gray rhyolite and tuff;
- Quaternary (Q): alluvial-mire facies loose deposits, 5–20 m thick.

Intrusive rocks are mainly Hercynian syenogranite ($\eta\gamma$) and Yanshanian granodiorite ($\gamma\delta$), intruding Paleozoic strata in stocks.

Three dominant structures control mineralization: the NE-trending ore-controlling structure, which controls the spatial distribution of the Bacheli gold vein; the NW-trending rock-controlling structure, which aligns with the copper ore belt, forming 50–200 m wide fracture alteration zones; and the near-EW-trending concealed faults, for which geophysical inversion indicates deep steep fault zones, potentially serving as deep fluid channels.

3. Prospective Prediction Methods and Achievements in Far-Field Areas

3.1. Data Sources

The data were collected from the 1:50,000 soil geochemical, phase-induced polarization and high-precision magnetic surveys conducted by the Institute of Geophysics and Geochemistry, Chinese Academy of Geological Sciences, in the Fudiyingzi–Bacheli area over the past few years. The surveyed area is approximately 340 km².

3.2. Soil Geochemical Analysis

Based on 2132 soil samples collected at a density of 5 samples/km², water sieving was used to remove fine particles and reduce the impact of carbonate and clay-adsorbed elements in forest–meadow areas on the geochemical field [19]. The samples were analyzed by a certified laboratory for 18 elements (e.g., Cu, Au, and Mo), with detection limits from ppb (Au and Hg) to ppm (Cu and Zn).

3.2.1. Single-Element Anomaly Delineation

This study used the content data of 18 elements from soil samples collected across the entire area. The anomaly threshold was determined using the mean-standard deviation method [20–22], combined with the geochemical field characteristics of the study area, through the following steps:

(1) Remove data points greater than or less than three standard deviations from the mean.
(2) Calculate the mean ($\overline{X}$) and standard deviation (S_0) of the remaining data.
(3) Determine the lower anomaly limit for each element.

$$T = \overline{X} \pm 2S_0$$

The calculated lower limits were used to map the geochemical anomalies of different elements. The main ore-forming elements Cu, Au, and Mo exhibit the following anomaly characteristics (Figure 2):

- Cu anomalies are predominantly concentrated in altered basalt (P_1d) in the northeastern region and crystal debris tuff of the Honghu Tuhe Formation (C_1hn) in the central-southern regions, showing spatial coupling with the copper-bearing Dashizhai Formation;
- Au anomalies are distributed in three key areas: (1) concentrated in the Dashizhai Formation (P_1d) and its surroundings in the northeast, where they correlate with the copper-bearing formation; (2) distributed along the contact zone between the Honghu Tuhe Formation and syenogranite in the southwest; and (3) widely dispersed across the Wudaoling Formation (P_2w), Guanghua Formation (K_1gn), and granodiorite ($\gamma\delta$) in the southeast, forming multiple concentration centers with the Bacheli gold deposit located at the anomaly center;
- Mo anomalies are sporadically distributed throughout the area but overlap with Au anomalies only in the southeastern region. Notably, a known molybdenum ore body in this region has a Late Paleozoic ore-forming age, suggesting multiple hydrothermal mineralization events.

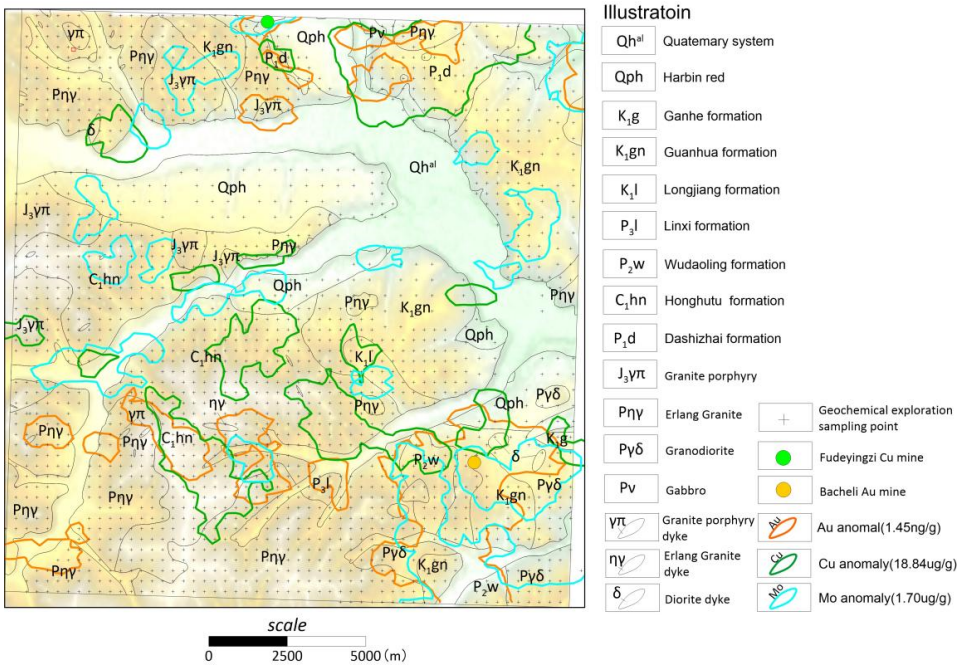


Figure 2. Geochemical anomaly distribution map of the main ore-forming elements Cu, Au, and Mo in the study area.

3.2.2. R-Type Cluster Analysis

To elucidate the element associations and correlations in this area, an R-type cluster analysis using Pearson correlation coefficients was conducted on the element content matrix. The analysis revealed three distinct groups (Figures 3 and 4):

1. MgO–Cr–Ni (R = 0.75–0.85) shows a high Pearson correlation coefficient, representing a typical rock-forming element combination associated with basic-ultrabasic rocks. Cu–Zn–Fe_2O_3 (R = 0.6–0.7) forms another group, where Cu–Zn is an important indicator for volcanic sedimentary copper deposits, while Fe_2O_3 suggests hematite association [9].
2. Au–Ag–As–Sb–Hg exhibit moderate correlation ($R \approx 0.4$–0.6), reflecting epithermal gold deposit characteristics; Au–Hg has strong correlation (R = 0.63), possibly indicating deep concealed mineralization; and As–Sb form an independent group showing secondary halo diffusion.
3. Mo is isolated ($R < 0.1$), likely related to Yanshanian granodiorite porphyry or independent hydrothermal channels. Combining cluster analysis results with the established prospecting model, significant geochemical anomalies closely linked to mineralization are evident in the study area.

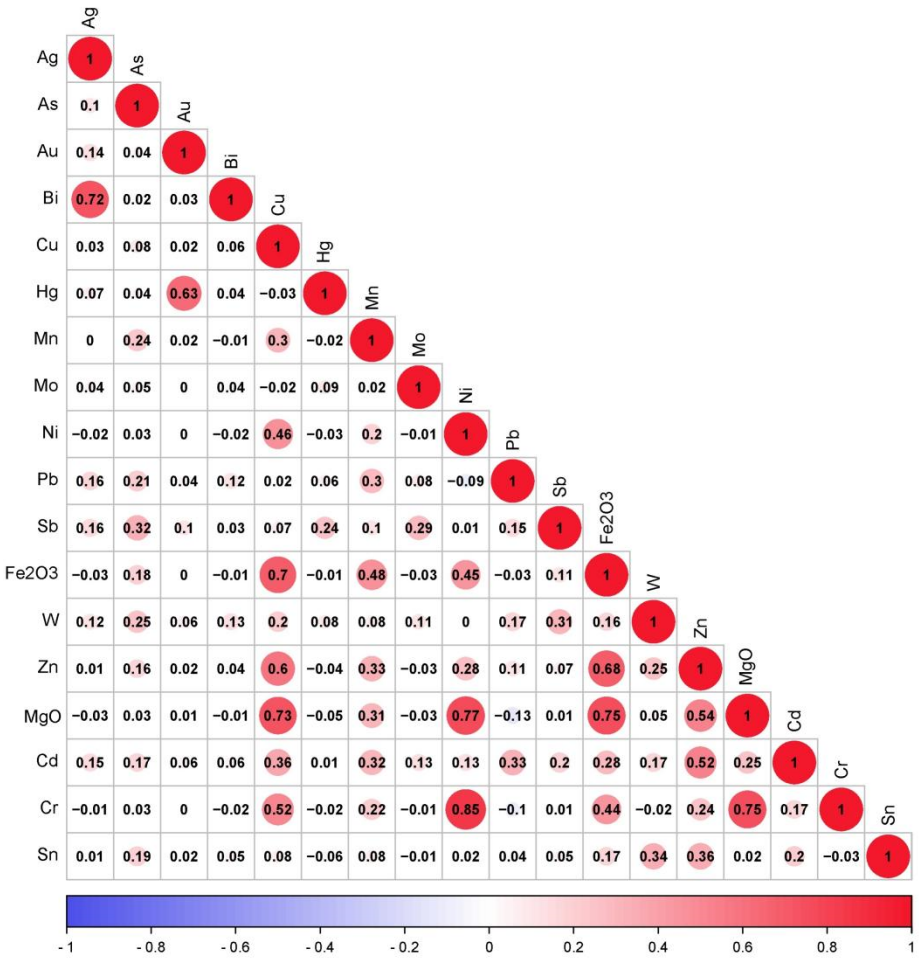


Figure 3. Matrix of element correlation coefficients.

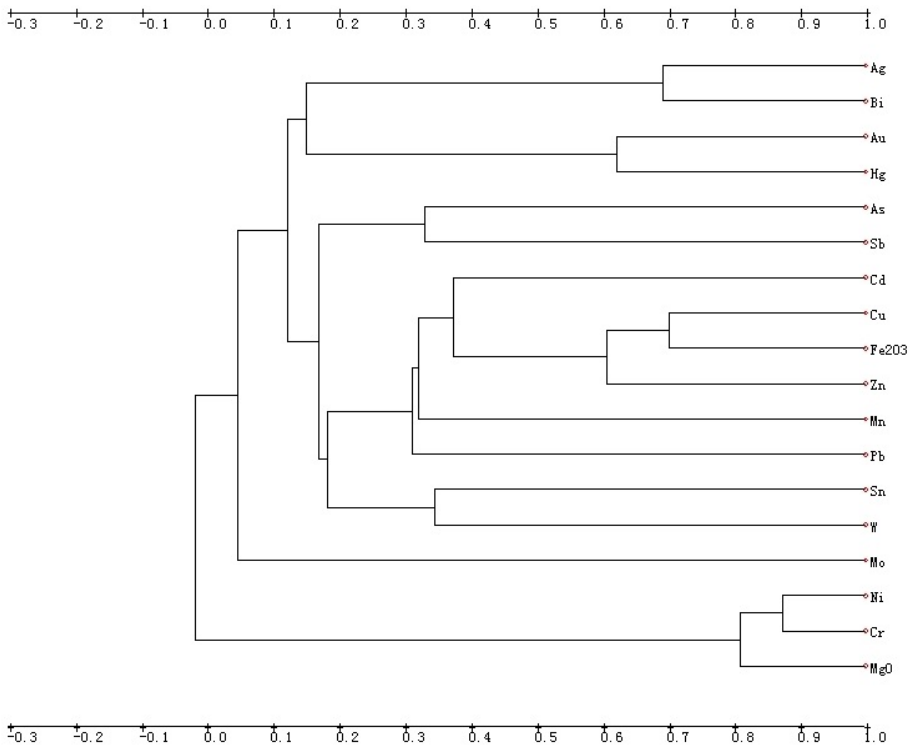


Figure 4. Dendrogram of R-type cluster analysis for elemental correlations.

3.3. Phase-Induced Polarization Analysis

Sulfides are characterized by a low resistivity and high polarization rate, which makes them ideal for investigating the geophysical responses associated with mineralization [23–27]. The FX-1(Produced by the Institute of Geophysical and Geochemical Exploration, China Geological Survey) amplitude-phase meter was employed to measure phase-induced polarization. This portable device features strong anti-interference capabilities and is capable of simultaneously measuring time-domain- and frequency-domain-induced polarization, providing both resistivity and apparent phase parameters in a single observation. The apparent phase parameters represent the rock's induced polarization effect, akin to traditional polarization rate parameters [28,29]. Area exploration was carried out with a survey line spacing of 500 m and point spacing of 100 m, adhering to DZ/T0070-93 „Technical Specifications for Time-Domain Induced Polarization Method". A dipole–dipole array configuration (AB = MN = a = 100 m, isolation factor n = 1) was utilized at a fixed working frequency of 0.25 Hz. The mean square relative error for apparent resistivity was ±7.60%, while the total mean square error for the apparent phase was ±0.63 milliradians.

Based on the apparent resistivity distribution and rock (mineral) physical parameters, the study area is divided into low-apparent-resistivity zones (<800 Ωm) and high-apparent-resistivity zones (≥800 Ωm). The geological map shows that low-apparent-resistivity zones mainly expose the Lower Cretaceous Guanghua Formation and Quaternary strata, while other strata and intrusive rocks are predominantly in high-apparent-resistivity zones (Figures 5 and 6). Metal sulfides typically exhibit low-apparent-resistivity and high-polarization characteristics. From the apparent phase contour map, nine significant high-phase anomalies (1–9) and six weak-phase anomalies (I–VI) were identified. Anomalies 1, 2, 4, 8, and VI occur in low-apparent-resistivity areas, while anomalies 3, 5, 6, 7, I, II, and IV are in high-apparent-resistivity zones, with some localized in low-apparent-resistivity zones within a high-resistivity background (Figures 5 and 6). High-phase and low-apparent-resistivity areas may indicate favorable metal sulfide deposit targets. However, high-phase anomalies could result from carbonaceous strata (e.g., Wudaoling Formation in the south-

east) or non-mineralized dark minerals, and low apparent resistivity might stem from non-mineralized faults. A comprehensive analysis of geological and geochemical data is required in order to exclude non-mineralized anomalies.

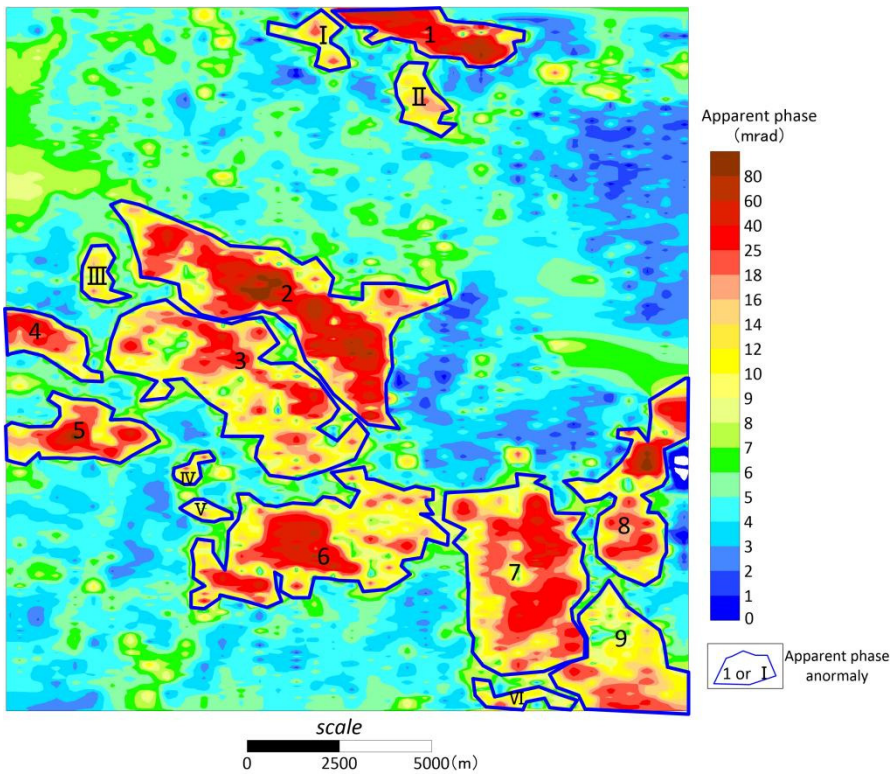


Figure 5. Distribution of apparent phase anomalies in the study area.

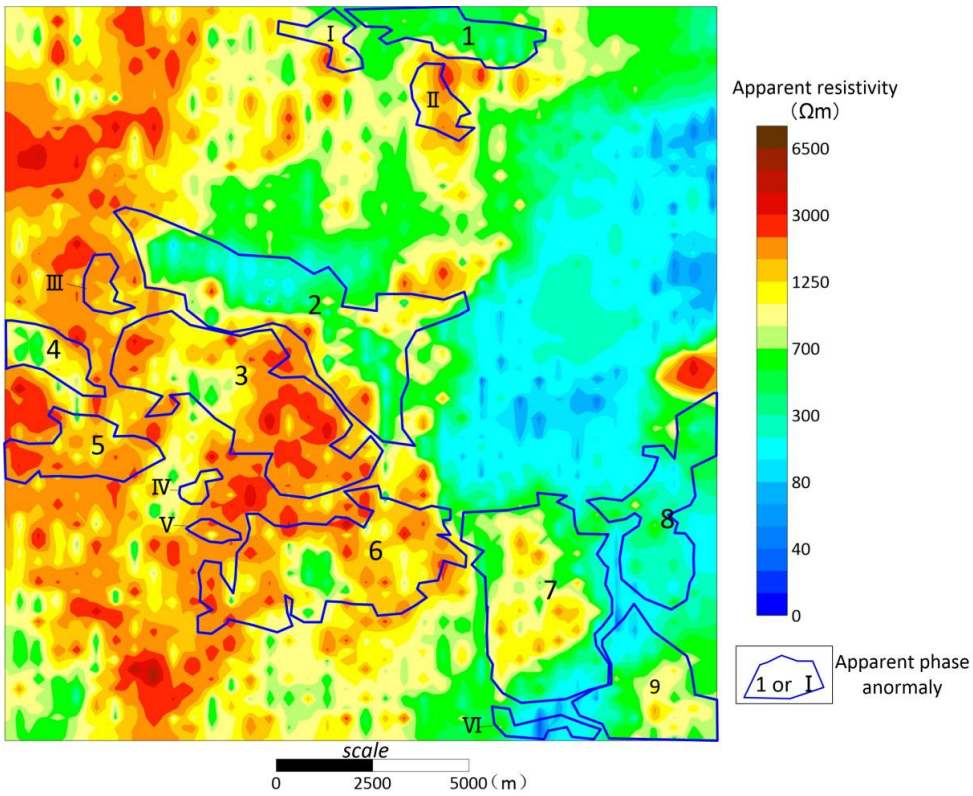


Figure 6. Distribution of apparent resistivity in the study area.

3.4. Ground High-Precision Magnetic Method

Magnetic exploration, which relies on the magnetic differences among rocks, minerals, and geological targets, is a geophysical technique used to investigate structural features and rock distribution, and delineate mineralization zones [30–34]. In the study area, data acquisition was conducted using a GSM-19T (Produced by GEM Systems Inc., Markham, Canada) proton magnetometer. The survey grid aligned with the phase-induced polarization grid. The survey adhered to the "Technical Regulations for Ground High-Precision Magnetic Survey" (DZ0071-93), achieving an accuracy of ±1.1 nT.

Magnetic anomaly (△T) data were processed using magnetic declination to improve the correspondence between magnetic bodies and anomalies [35,36] (Figure 7). The results show a significant strong magnetic anomaly on the north side of the study area, associated with ultrabasic–basic volcanic rocks. The Fudiyingzi copper mine is located near this anomaly and correlates with these strata, indicating a favorable area for this type of copper deposit. The Lower Cretaceous Guanghua Formation exhibits strong magnetism, while diorite ($\eta\gamma$) and granitic porphyry ($\gamma\pi$) areas typically show medium magnetic intensity. The Lower Carboniferous Honghutu Formation (C_1hn) shows no or weak magnetism.

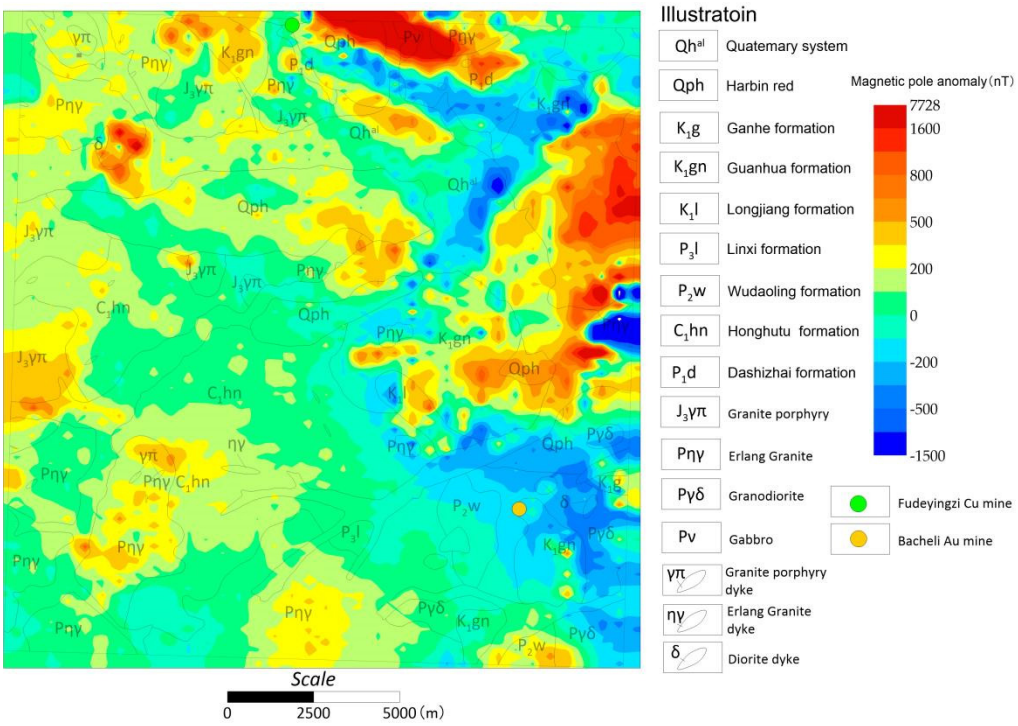


Figure 7. Overlay of ground RTP magnetic anomalies and geological information.

To enhance structural identification, gradient band filtering was applied to process magnetic declination anomalies. This nonlinear filtering technique divides the weighted area into eight subdomains, calculates the mean square deviations, and selects the subdomain with the minimum deviation as the filter reference, optimizing the gradient band anomaly extraction [37,38]. We implement this filter as follows:

1. Calculate the mean and variance of anomalies within each subdomain, specifically:

$$\delta_i = \sqrt{\sum_{j=1}^{n} (\overline{g_i} - g_i(j))/m_i}$$

In the formula, m_i denotes the number of anomalous points in the *i*region, $\overline{g_i}$ represents the average anomaly in the i region, $g_i(j)$ is the outlier at the*j*point within the ith region i, and δ_i corresponds to the variance of anomalies in the i region.

2. Select the smallest $\delta_i(\delta_{\min})$.
3. Use the mean anomaly value from this subdomain as the processing result.
4. Slide the window to the next point and repeat steps 1–3.

The magnetic gradient band filtering and enhancement technique significantly amplifies the magnetic gradient, improves the boundary resolution, accurately defines the magnetic body boundaries, and sensitively identifies the concealed faults and lithologic contacts. The calculation results reveal multiple NE- and NW-trending linear structures in the study area, with additional E–W and NNE trends in the central–northern region (see Figure 8). While not all inferred linear structures are faults, their spatial distribution aligns with regional structural patterns. These structures and their intersections may represent favorable mineralization zones. Further investigation is required in order to confirm whether these linear features correspond to faults.

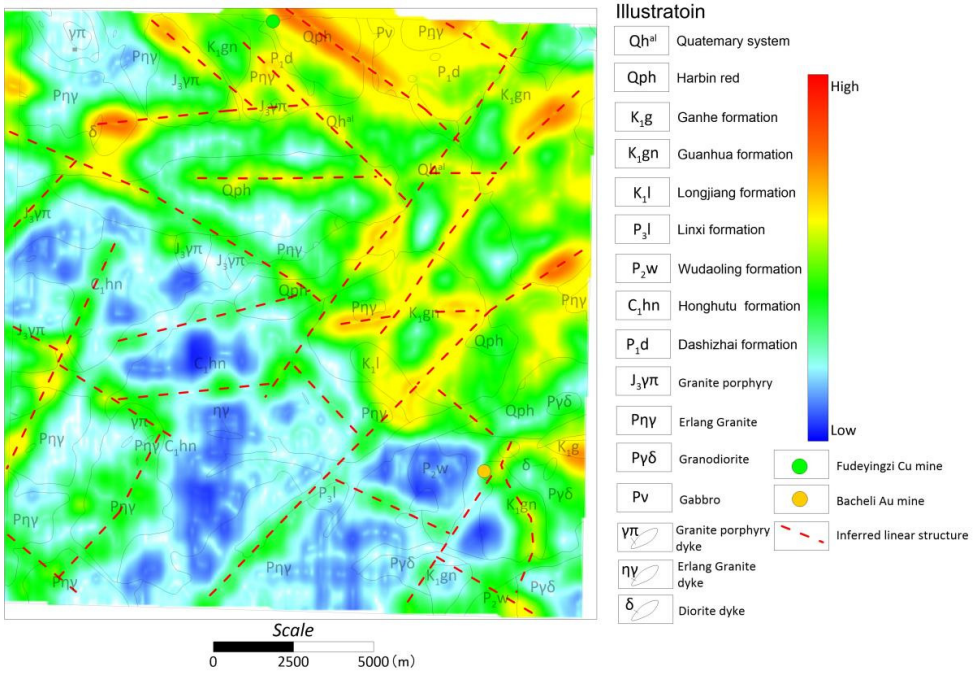


Figure 8. Stepwise band-filtered enhancement of ground magnetic anomalies and inferred linear structural distribution.

3.5. Typical Deposit and Prospecting Model

3.5.1. Research on Typical Deposit

The Fudiyingzi copper deposit formed in the Late Carboniferous during the subduction of the Paleo-Asian Ocean. Mineralization occurred at approximately 310.5 Ma, slightly later than the volcanic eruption of host rocks (amphibolite, and plagioclase amphibolite). The ore bodies are controlled by NEE-trending faults and near-east–west and northwest structures, hosted in the Dashizhai Formation's metamorphic volcanic rocks. The lithology includes basalt, dacite, intercalated limestone, sandstone, and mudstone lenses, representing submarine volcanic–sedimentary construction. The main ore-bearing rock is pyroxene–amphibolite (original ultrabasic volcanic rocks). The ore body conforms to the stratigraphy, with layered upper parts and vein-disseminated lower sections. The ore minerals include chalcopyrite, sphalerite, pyrite, and pyrrhotite, with trace native gold and silver. The internal sulfur content exceeds 20%, copper >3%, while the external sulfur is <20%,

copper 1.5%3%. The wall rock alteration shows zoning from chloritization–sericitization–silicification to silicification–carbonatization, with chloritization and silicification closely linked to mineralization. Sulfur isotopes ($\delta^{34}S$ = -1.5‰ to +4.6‰) indicate a magmatic sulfur source from basaltic rocks. The ore-forming fluid is a mix of magmatic water and heated seawater (temperature 189–392 °C, and pressure 15.4–26.9 MPa), forming at a 1.5–2.6 km depth beneath the seafloor. This is a typical volcanic hydrothermal exhalative–sedimentary copper deposit [9,39–42].

The Bacheli gold deposit is located in the southeast of the study area. The previous research on it is relatively weak, but the available data show that it has the characteristics of a low-sulfidation epithermal gold deposit [8,18,24,39]. The deposit is situated in the NE-trending epithermal gold mineralization belt, and its geological background for mineralization is consistent with that of the known deposits in this belt. The mineralization is temporally and spatially closely associated with the Mesozoic intermediate-acidic magmatic rocks, and the magmatic activity provides the heat source and part of the material for mineralization. The ore bodies are hosted in the alteration zones of the inner and outer contact zones of the diorite porphyry, granitic porphyry, and quartz porphyry dikes or the Mesozoic granitic rocks and volcanic rocks. Vertically, they are controlled by the NE-trending fault system under the background of the Mesozoic–Cenozoic active continental margin subduction zone. The NE-trending structural fracture zones and their secondary fractures are the main channels for the migration of ore-bearing fluids and the precipitation of ore minerals. The silicification–pyritization–sericitization alteration assemblage is significantly positively correlated with the intensity of gold mineralization, revealing its epithermal-low-sulfur-type mineralization attribute.

3.5.2. Prospecting Model

The prospecting model for copper and gold deposits in the study area integrates geological elements with geophysical and geochemical anomalies. For volcanogenic massive sulfide (VMS) deposits, host rocks include pyroxene amphibolite and hornfels-altered basalt. These are delineated using MgO–Cr–Ni geochemical associations, high magnetic anomalies, and a medium resistivity with high polarization. The controlling structures are EW- and NW-trending faults, identified via magnetic methods. The mineralized bodies are marked by Cu–Zn–Au geochemical associations and a low resistivity with high polarization. For hydrothermal gold deposits, the host rocks consist of intermediate-acidic dikes (diorite porphyry and granitic porphyry) and fractured altered rocks. These are identified through weak magnetic anomalies and a medium resistivity with high polarization. The controlling structures are NE-trending faults, also interpreted magnetically. The mineralized bodies are characterized by Au–Ag–As–Sb–Pb–Zn associations and a low resistivity with high polarization, reflecting epithermal low-sulfidation processes. This model combines geological mapping, geochemical zoning, and geophysical characteristics to spatially locate mineralization elements and assess the intensity, providing a quantitative basis for regional exploration (Table 1).

Table 1. Geological, geochemical, and geophysical prospecting models for copper and gold deposits.

Category	Volcanic Exhalative-Sedimentary Copper Deposit	Hydrothermal Gold Deposit
Host Rock	Geological: Hornblende amphibolite, hornfelsed basalt, felsic hornfels Geochemistry: MgO–Cr–Ni anomaly Geophysics: High magnetic, medium resistivity with high polarization	Geological: Diorite porphyry, granitic porphyry, quartz porphyry, altered/ fractured rocks Geophysics: Weak magnetic, medium resistivity with high polarization

Table 1. *Cont.*

Category	Volcanic Exhalative-Sedimentary Copper Deposit	Hydrothermal Gold Deposit
Controlling Structures	Geological: NE–SW- and NW-trending faults	Geological: NE-trending faults
	Geophysics: Magnetic inferred linear structures	Geophysics: Magnetic inferred linear structures
Mineralization Alteration	Silicification, chloritization, sericitization, pyritization, carbonatization	Silicification–pyritization–sericitization alteration assemblage
	Mineral Assemblage: Chalcopyrite, sphalerite, pyrite, pyrrhotite, trace native gold.	Mineral Assemblage: Pyrite, limonite, sphalerite, galena, gold minerals
Ore Characteristics	Geochemistry: Cu–Zn–Au anomaly	Geochemistry: Au–Ag–As–Sb–Pb–Zn anomaly
	Geophysics: Low resistivity with high polarization	Geophysics: Low resistivity with high polarization

3.6. Prediction of Prospective Mineralization Areas

Based on the study of typical mineral deposits and the established prospecting model, combined with a geophysical and geochemical data analysis, four prospective exploration areas were identified (Figure 9). The details are as follows.

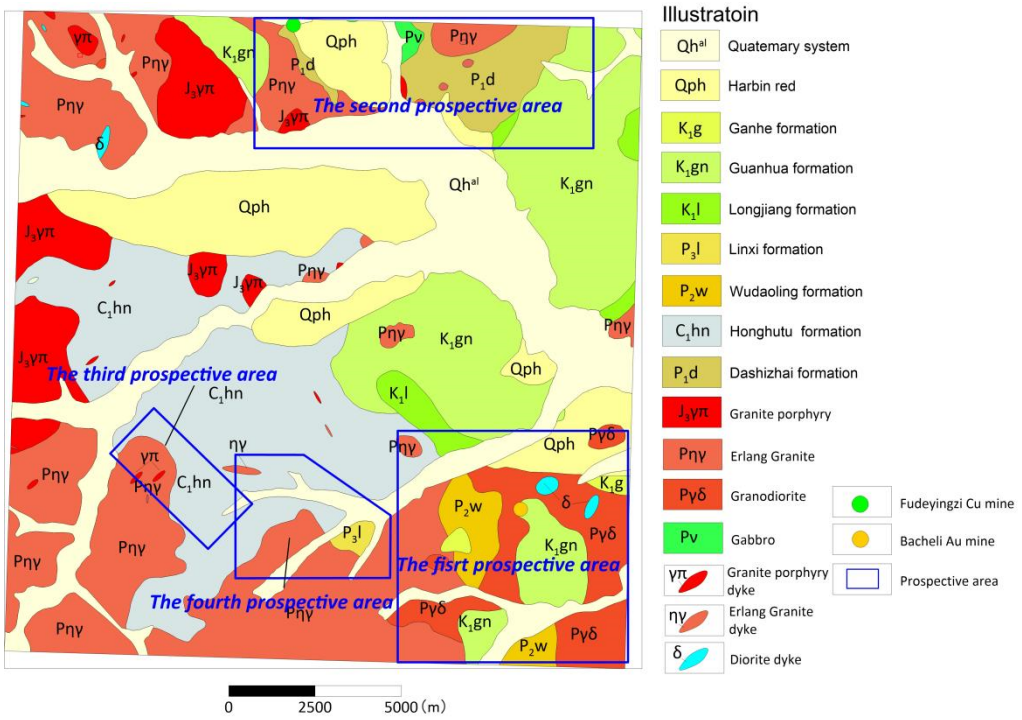


Figure 9. Map illustrating the distribution of prospective areas on the geological map of the study region.

The first prospective area is located in the southeast of the study region, covering approximately 36 km². It includes strata and intrusive rocks such as K_1gn, K_1g, P_2w, $P\gamma\delta$, and δ, at the intersection of the northeast and northwest linear structures. The magnetic anomalies are weak (90% < 200 nT), with apparent resistivity values low in the east (<800 Ωm) and moderate in the west (800–1100 Ωm). The geochemical anomalies show complex element combinations: Au, Ag, As, Sb, and Hg form one group, while W, Mo, Pb, and Bi form another (Figure 10). These correspond to the hydrothermal gold deposit model and highlight this area as a key target for further Au and Mo exploration.

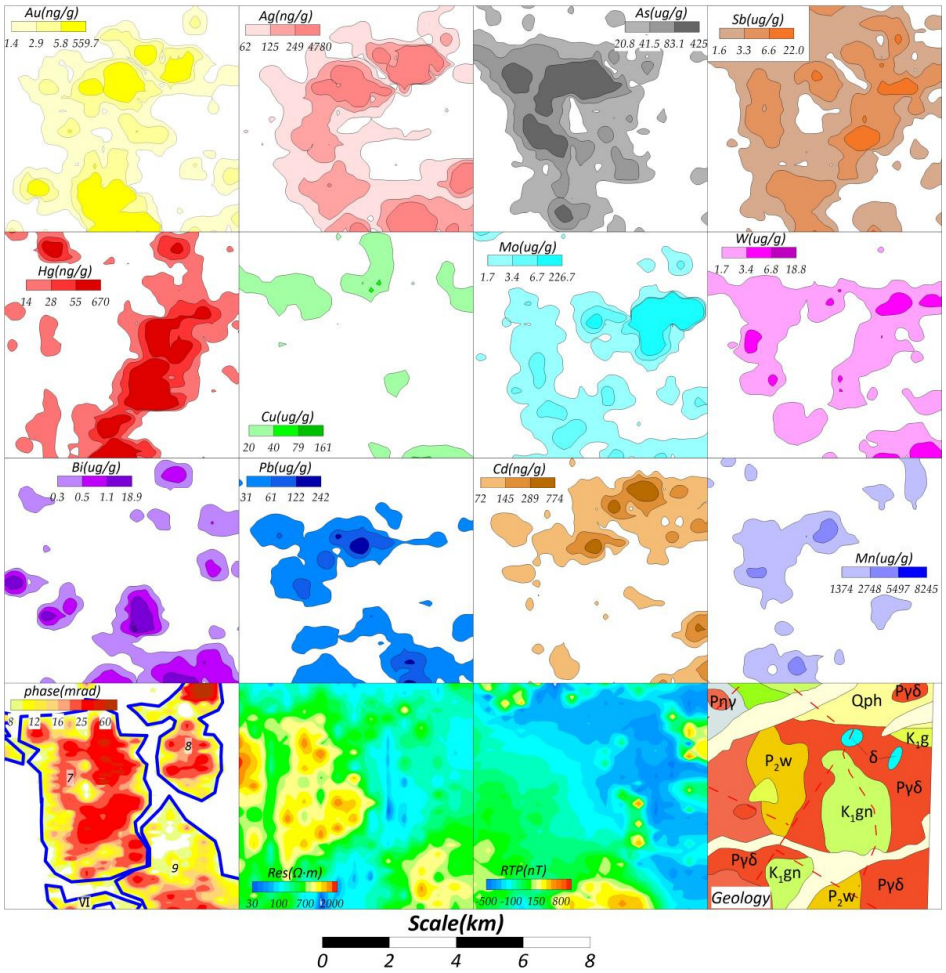


Figure 10. Geophysical, geochemical, and geological analysis map of the first prospective area.

The second prospecting area, located in the northern part of the study area (approximately 30 km²), features regional strata and intrusive rocks including P_1d, K_1gn, Qph, and $P\eta\gamma$, with sporadic outcrops of $J_3\gamma\pi$ and $P\nu$. Three northwest-trending structures intersect with northeast-trending structures on the east side and east–west-trending structures on the west side. Apparent phase anomalies (1, I, and II) correspond to low, low, and medium apparent resistivity values, respectively. Anomaly 1 also aligns with a high magnetic anomaly trending northwest, while anomalies I and II align with weak magnetic anomalies of the same trend. The geochemical anomalies of Cu, Zn, Au, Cd, Fe_2O_3, MgO, Cr, Ni, etc. (Figure 11) match well with the volcanic-rock-type copper deposit model, suggesting the potential for the further exploration of polymetallic deposits such as Cu and Au.

The third prospecting area, located in the central–southern part of the study area (approximately 10 km²), features strata and intrusive rocks including C_1hn, $P\eta\gamma$, and $\gamma\pi$. Northeast and northwest structures intersect here. Magnetic anomalies reach approximately 400 nT, with apparent phase anomalies IV, V, and part of No. 6. Anomaly IV shows a medium–low resistivity, while others show a medium–high resistivity. Four Au anomalies are distributed in a northwest bead-like pattern, with two extreme points and a peak value of 36.43×10^{-9}. This area also exhibits Cu, Zn, and Cd anomalies (see Figure 12), potentially indicating metal enrichment during sulfide mineralization. Although the lithology differs from known models, the anomaly combination correlates with volcanic-rock-type copper deposits, making it a favorable area for Cu–Au exploration.

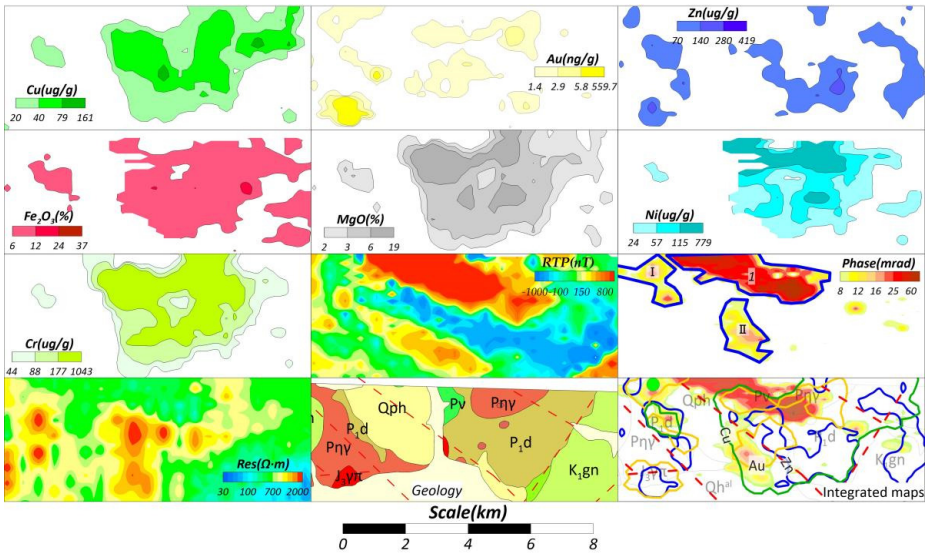


Figure 11. Geophysical, geochemical, and geological analysis map of the second prospective area.

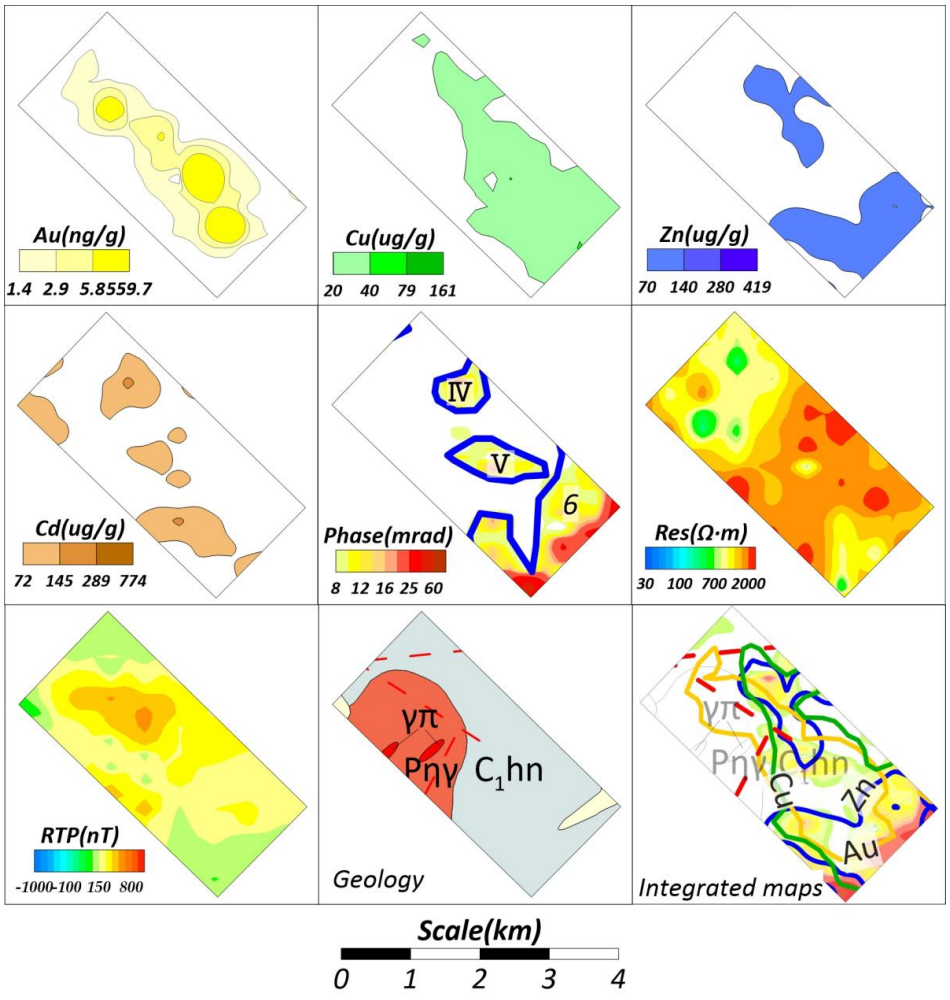


Figure 12. Geophysical, geochemical, and geological analysis map of the third prospective area.

The fourth prospecting area, located in the central–southern part of the study area (approximately 15 km²), features exposed strata and intrusive rocks including C_1hn, $P\eta\gamma$, and sporadic P_3l. Soil measurement anomalies are primarily distributed along the northeast contact zone. The anomaly element combination includes Au, As, Ag, Zn, Pb, Sn, W, and Mo, with the Au, Ag, and As anomalies showing a good superposition. At the main anomaly

sites, a high-apparent-phase No. 6 anomaly occurs, characterized by a low resistivity in a high-resistance background. Magnetic anomalies show a gently sloping low-background trend in the northeast direction, adjacent to the northeast linear structure inferred from the magnetic data (Figure 13). This area is favorable for exploring hydrothermal Au deposits.

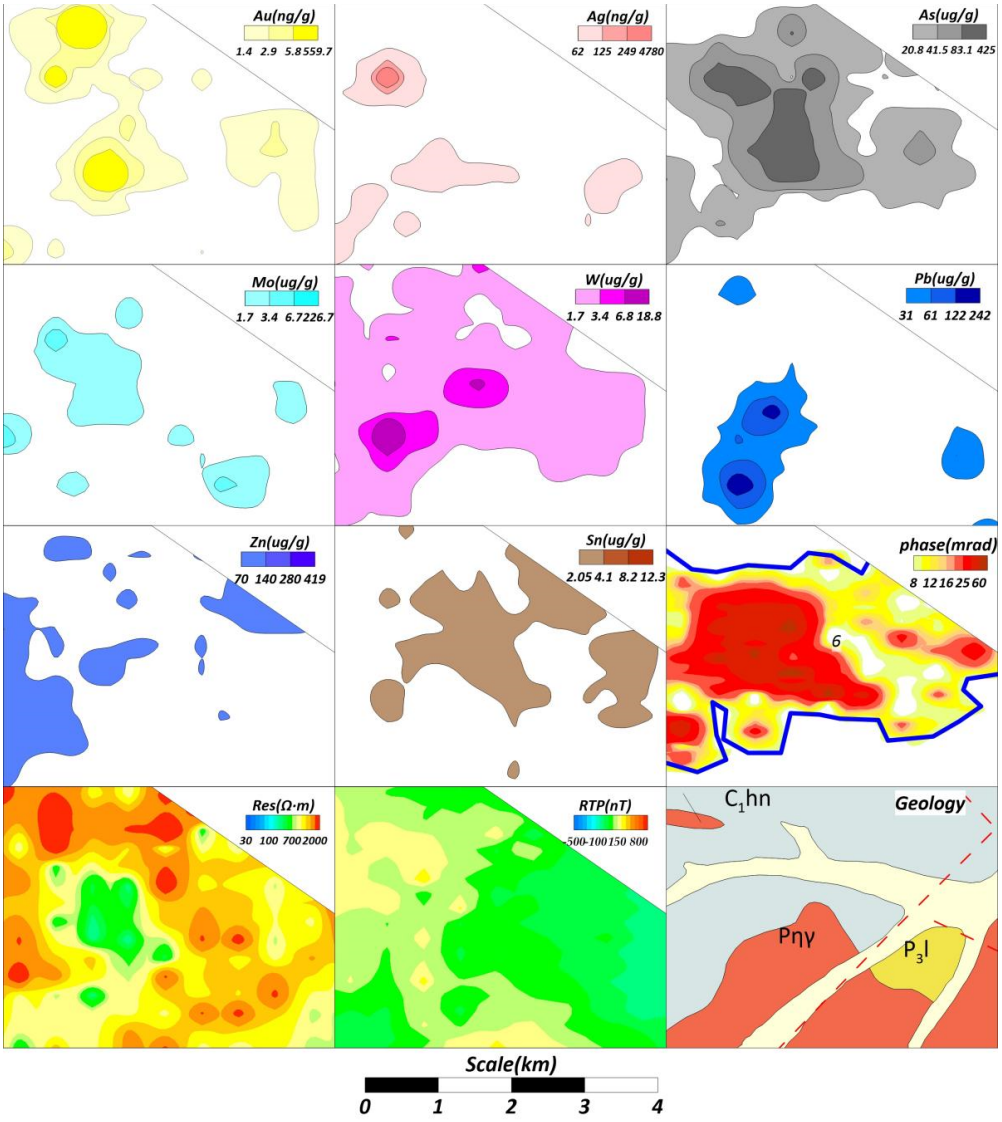


Figure 13. Integrated geophysical, geochemical, and geological analysis map of the fourth prospective area.

4. Discussion

The VMS deposit is an important type of deposit formation that is widely distributed around the world. It mainly forms in the submarine volcanic environment and is widely distributed in various mountain-building belts. VMS deposits worldwide can be classified by chemical composition into the Cu–Zn, Zn–Cu, and Zn–Pb–Cu types. Based on the tectonic environment and host volcanic rock types, they are further categorized as the Noranda, Cyprus, black ore, and Besshi types. The Noranda-type deposit was formed in the subduction zone at the edge of a subducting plate. The host rock of the deposit is mainly basic–acidic double-peak volcanic rocks, and the main mineral composition is Cu–Zn. The Cyprus-type deposit is located at the spreading mid-ocean ridge. The host rock includes peridotite and felsic basalt, and the main minerals are Cu. The black-ore-type deposit is located in the island arc or post-arc basin, and the host rock is double-peak basalt,

with the main minerals being Cu–Pb–Zn. The Besshi-type deposit is distributed in the fore-arc trench, and the host rock is basic rock and felsic basalt, with the main minerals being Cu–Zn [9,10,41]. The Noranda-type deposits are mainly distributed in the Noranda ore concentration area in Canada. In China, there are mainly the Hongtoushan copper mine in Liaoning Province and the Asheller copper mine in Xinjiang. In Europe and Africa, their distribution is relatively scarce. The resource potential of the Noranda-type deposits is still concentrated in the edge of the ancient craton and the volcanic rock sequences of the active orogenic belt. In China, in the northern part of Xinjiang (Altay, East Tianshan), and in the Central Asian orogenic belt, due to multiple periods of volcanic activity, it is a key exploration area for future VMS-type copper deposits. The study area is located in the eastern section of the Central Asian orogenic belt, with multiple periods of volcanic activity, and it is one of the regions with exploration potential.

The Fudiyingzi copper deposit is a Cu–Zn VMS deposit with Noranda-type characteristics: it contains Cu and Zn as primary elements, with Au enrichment, but lacks significant Pb mineralization typical of Hokuroku deposits. This aligns with the geochemical anomalies in the second and third prospective areas of the study region. The second prospecting area shows significant geophysical and geochemical anomalies consistent with the established model. Despite the Quaternary cover obscuring Ni-, Cr-, and MgO-related mafic–ultramafic anomalies, deep volcanic rocks still hold substantial exploration potential. It is recommended to use deep geophysical methods (e.g., controlled-source audio-frequency magnetotellurics) and penetrating geochemistry to detect concealed ore bodies.

Epithermal gold deposits form in shallow environments (<1.5 km) and are closely linked to volcanic-intrusive rock systems. Mineralization typically occurs at 200–300 °C (rarely <200 °C or >350 °C) under low pressure (10–50 MPa) [42]. The Bacheli gold deposit, despite lacking systematic fluid temperature and pressure data, exhibits typical epithermal characteristics: silicification, pyritization, sericitization, NE-trending ore-controlling structures, and Yanshanian mineralization age. Six gold ore bodies have been identified in the southeastern first prospecting area, aligning with a geology–geochemistry–geophysics integrated model (weak magnetic anomalies, low resistivity/high polarization, and Au–Ag–As–Sb–Pb–Zn element associations), confirming its reliability. Future work should focus on fluid inclusion and isotope studies to refine the ore-forming mechanism and enhance deep/peripheral exploration for resource expansion.

A single prospecting method has limitations. Relying solely on geochemical anomalies (e.g., Cu–Zn–Au–Ag) for prediction while ignoring the polarization effect of mineralized bodies can overestimate the target area (see Figure 2), delineating a much larger prospective zone than the actual mineralization boundary. Conversely, selecting targets based only on geophysical anomalies (e.g., apparent phase anomalies) may introduce non-mineral interference from the carbonaceous strata or Ganhe Formation basalt (e.g., anomaly No. 2). Research shows that integrating geology, geochemistry, and geophysics effectively reduces interference by constraining mineral-forming lithologies through geological mapping, defining mineralization ranges via geochemical element zoning, and incorporating geophysical field characteristics, ultimately achieving accurate target delineation.

5. Conclusions

This study systematically predicted the copper and gold polymetallic mineralization potential in the Fudiyingzi–Bacheli area of Heilongjiang Province using multi-source information fusion technology, reaching the following conclusions:

(1) Two mineralization models—"volcanic-rock-type copper deposit" and "hydrothermal-type gold deposit"—were established based on typical deposits. These models clar-

ified the key indicators and geophysical/geochemical anomalies for exploration, providing theoretical guidance.

(2) A "geology–geophysics–geochemistry–GIS" collaborative model was constructed using 1:50,000 soil geochemistry, phase-induced polarization, and high-precision magnetic data. This integrated approach improved target selection efficiency.

(3) Four prospective areas totaling ~91 km² were identified in the southeast, north, and central–south of the study area, each with distinct geological features and mineralization anomalies, marking key exploration zones.

(4) The "geology–geochemistry–geophysics" prediction model provides a scientific basis for regional exploration and serves as a technical demonstration for similar concealed ore body exploration.

(5) Despite the achievements, limitations remain. Advanced techniques (e.g., controlled-source audio-frequency magnetotellurics) and penetrating geochemistry are recommended for deeper mineralization insights. Ground surveys and drilling should also be strengthened for new discoveries.

In summary, this study offers new ideas and methods for copper and gold polymetallic exploration in the Fudiyingzi–Bacheli area, with significant theoretical and practical implications.

Author Contributions: Conceptualization and software, L.C.; methodology, H.W.; formal analysis, L.C.; investigation, L.C.; resources and data curation, L.C.; writing—original draft preparation, H.W.; visualization, L.C. and W.D.; supervision, H.W. and C.S.; project administration, L.C.; funding acquisition, L.C.; software, C.S.; validation, C.S. and W.D.; writing—review and editing, X.C. All authors have read and agreed to the published version of the manuscript.

Funding: This study was funded by the China Geological Survey (DD20230701505,1212010781025).

Data Availability Statement: The data presented in this study are not publicly available due to privacy and ethical restrictions. However, interested researchers can request access to the original observational data by contacting the corresponding author.

Conflicts of Interest: The authors declare no conflicts of interest.

References

1. Tang, J.X.; Yang, H.H.; Chen, H.J.; Li, F.Q.; Wang, C.Y.; Liu, Q.P.; Zhang, Q.; Zhang, R.K.; Yu, L.R. Potential and future direction for copper resource exploration in China. *Green Smart Min. Eng.* **2024**, *1*, 127–131. [CrossRef]
2. Bai, C.L.; Xie, G.Q.; Liu, Y.; Chen, J.; Zhu, Q.Q.; Li, W. Implications of the newly discovered Triassic suites from the eastern segment in the giant Tongshan porphyry Cu deposit, northeast China. *Geosci. Front.* **2025**, *102034*, 1674–9871. [CrossRef]
3. Bai, C.L.; Xie, G.Q.; Zhao, J.K.; LI, W.; Zhu, Q.Q. Metallogenic characteristics and ore deposit model of porphyry copper epithermal gold system in the Duobaoshan ore field, eastern margin of the Central Asian Orogenic Belt. *Earth Sci. Front.* **2024**, *31*, 170–198.
4. Zhao, Z.H.; Zheng, W.Z.; Qu, H. Cu-Au mineralization and metallogenic regularity of Duobaoshan area, Heilongjiang Province. *Miner. Depos.* **2012**, *31*, 601–614.
5. Zhao, Z.H.; Qu, H.; Guo, Y. Metal logenic Rules and Prospecting Orientation of Gold Deposit in the Duobaoshan Area, Heilongjiang Province. *Geol. Resour.* **2011**, *20*, 89–95.
6. Zhang, S.; Ju, N.; Zhang, G.B.; Zhao, Y.D.; Ren, Y.S.; Liu, B.S.; Wang, H.; Guo, R.R.; Yang, Q.; Sun, Z.M.; et al. Geology and mineralization of the Duobaoshan supergiant porphyry Cu-Au-Mo-Ag deposit (2.36 Mt) in Heilongjiang Province, China: A review. *China Geol.* **2023**, *6*, 100–136. [CrossRef]
7. Pan, Z.D.; Hou, H.S.; Zhou, J.B.; Wei, F.; Zhang, X.Z.; Huang, S.Q.; An, D.Z.; Liu, W.Y.; Yang, J.; Guo, R. Crustal structure and Paleozoic metallogenic tectonic setting of the Duobaoshan ore district, NE China. *Ore Geol. Rev.* **2021**, *137*, 104290. [CrossRef]
8. Xu, G.H. Geological features and prospecting criteria of Bacheli gold-molybdenum deposit in Heihe city, Heilongjiang province. *Gold* **2008**, *29*, 15–19.
9. Nie, S.J. The Geological Characteristics and Genesis of the Fudiyingzi Cu Deposit in Heihe City, Heilongjiang Province. Master's Thesis, Jinlin University, Changchun, China, 2018.

10. Xiang, W.S.; Zhao, K.; Zeng, G.P.; Li, F.L.; Wang, J.X.; Hu, P.; Zhang, Z.C. Geology of VMS deposits in Northeast Africa and their research progress. *Geol. Bull. China* **2022**, *41*, 129–140. [CrossRef]
11. *DZ/T 0426-2023*; Specification for Geological Survey of Mineral Resources (1:50000). Geological Publishing House: Beijing, China, 2023.
12. Meng, F.W. The Study of Lithospheric Electrical Structure and Metallogenic Setting in the Northern Section of the Heihe-Hegenshan Suture. Ph.D. Thesis, Jinlin University, Changchun, China, 2023.
13. Jia, W.G.; Xin, H.T.; Li, Y.F.; Liu, Q.S.; Ha, D.M.; Xing, D.H.; Sun, Z.R.; Chen, S.W. The new round of prospecting breakthrough strategic action in northeast china: Deployment and reflection. *Geol. Resour.* **2024**, *33*, 403–416, 492.
14. Zhang, Y.F.; Guo, W.J.; Wu, G.X.; Zhao, H.G.; Wu, T.T. Prediction and verify of concealed orebody in Bacheli mining area and its periphery in Heihe of Heilongjiang. *World Geol.* **2012**, *31*, 85–92.
15. Han, Z.Z.; Liu, N.; Gong, F.Y.; Li, Y.S.; Li, Y.C.; Yao, L. Cu-Au Polymetallic Mineralization and Prospecting Direction in Duobaoshan-Daxintun Area, Heilongjiang. *Geol. Rev.* **2015**, *61*, 787–796.
16. Hao, Y.J.; Ren, Y.S.; Duan, M.X.; Tong, K.Y.; Chen, C.; Yang, Q.; Li, C. Metallogenic events and tectonic setting of the Duobaoshan ore field in Heilongjiang Province, NE China. *J. Asian Earth Sci.* **2015**, *97*, 442–458. [CrossRef]
17. Kong, M.; Yang, S.P. Preliminary research into the disturbed principle of organic material tocharacter of Supergene-Geochemistry in forest marsh andscape area. *Geophys. Geochem. Explor.* **2008**, *32*, 31–32.
18. Sun, Z.J. Multifractal Method of Geochemical Threshold in Mineral Exploration. *Comput. Tech. Geophys. Geochem. Explor.* **2007**, *29*, 54–57.
19. Chen, M.; Li, J.C. Problem and counter measure of recognition of geochemical background and anomaly problem. *Geol. Prospect.* **1999**, *35*, 25–29.
20. Chao, X.; GE, L.Q.; Luo, Y.Y. Comparison of multiple method to determine the geochemical anomalies in the lower limit. *Sichuan Nonferrous Met.* **2012**, *1*, 52–61.
21. Yin, Q.; Wang, K.; Tan, G.; Ji, Y.; Yang, H.; Chen, H.; Sun, Y.; Liu, Q.; Sun, T. Geophysical Characteristics of Low-Sulfide Epithermal Gold Mineralized Bodies—A Case Study of the Alinghe Mining Area on the South Bank of the Heilong River in China. *Minerals* **2025**, *15*, 47. [CrossRef]
22. Doyle, H.A. Geophysical exploration for gold—A review. *Explor. Geophys.* **1986**, *17*, 169–180. [CrossRef]
23. Fatehi, M.; Haroni, H.A. Geophysical signatures of the gold rich porphyry copper deposits: A case study at the Dalli Cu-Au porphyry deposit. *J. Econ. Geol.* **2018**, *10*, 639–675.
24. Hoschke, T.; Sexton, M. Geophysical exploration for epithermal gold deposits at Pajingo, North Queensland, Australia. *Explor. Geophys.* **2005**, *36*, 401–406. [CrossRef]
25. Seigel, H.O.; Johnson, I.; Hennessey, J. Different methodology: Geophysical aids to gold exploration. *Lead. Edge* **1984**, *3*, 32–35. [CrossRef]
26. Ye, S.M. Results of test surveys in three mining districts in Jiangxi Province with FX-1 amplitude-phase meter. *Geol. Explor.* **2003**, *39*, 31–35.
27. Zhu, C.H. Application of FX-1 phase meter in small scale geological survey. *Heilongjiang Land Resour.* **2011**, *5*, 75.
28. Abdelrahman, K.; El-Qassas, R.A.Y.; Fnais, M.S.; Andráš, P.; Eldosouky, A.M. Geological Structures Controlling Au/Ba Mineralization from Aeromagnetic Data: Harrat ad Danun Area, Saudi Arabia. *Minerals* **2023**, *13*, 866. [CrossRef]
29. Zhang, Z.; Li, Y.; Chen, L.; Zhang, Q.; Sun, Y. Deep Geological Structure Analysis of the Dongyang Area, Fujian, China: Insights from Integrated Gravity and Magnetic Data. *Minerals* **2024**, *14*, 837. [CrossRef]
30. Zhdanov, M.S.; Wan, L.; Jorgensen, M. Joint Three-Dimensional Inversion of Gravity and Magnetic Data Collected in the Area of Victoria Mine, Nevada, Using the Gramian Constraints. *Minerals* **2024**, *14*, 292. [CrossRef]
31. Meng, Q.F.; Ma, G.Q.; Li, L.L.; Wang, T.T.; Li, Z.R.; Wang, N.; Li, J.G. Joint Inversion of Gravity and Magnetic Data with Tetrahedral Unstructured Grid and its Application to Mineral Exploration. *IEEE Trans. Geosci. Remote Sens.* **2023**, *61*, 5915514. [CrossRef]
32. Essa, K.S.; Abo-Ezz, E.R.; Anderson, N.L.; Gomma, O.A.; Elhussein, M. Magnetic inversion approach for modeling data acquired across faults: Various environmental cases studies. *Acta Geophys.* **2024**, *72*, 1819–1845. [CrossRef]
33. Bao, S.C. The application of reduction to the pole magnetic anomaly approximation to determining the buried depth of isometric magnetic bodies. *Geophys. Geochem. Explor.* **2017**, *41*, 98–101.
34. Xie, R.K.; Xiong, S.Q.; Duan, S.L.; Wang, J.L.; Luo, Y.; Wang, P.; Duan, R.; Liu, H.J.; Fan, Z.G. Estimating total magnetization direction of magnetic sources by using airborne vector magnetic date. *Chin. J. Geophys.* **2021**, *64*, 3368–3378.
35. Yan, J.L.; Hu, W.B.; Yao, C.L. Filtering enhancement of gravity and magnetic data in the dense ladder-like zone. *Prog. Explor. Geophys.* **2006**, *29*, 102–103.
36. Xia, L.Y.; Wu, H.N.; Bo, G.J.; Hou, B.N. Research on enhancing weak signal technology and recognition of linear structures using aerial-magnetic data in the Qaidam Basin. *Prog. Geophys.* **2008**, *23*, 1058–1062.
37. Cai, W.Y. Metallogenesis of Copper-Molybdenum-Gold Polymetallic in the Duobaoshan Orefield, Heilongjiang Province. Ph.D. Thesis, Jilin University, Changchun, China, 2020. [CrossRef]
38. Zhang, J.R.; Chen, H.; Ren, J.P. Mineral Resource Assessment Methods Comparison and Its Development Trend Discussion. *Northwest. Geol.* **2023**, *56*, 292–305. [CrossRef]

39. Mao, G.W.; Cao, L.; Yan, X.P.; Sun, W.H.; Zhu, J.L.; Wang, B.T. A review of research on epithermal gold deposits. *Contrib. Geol. Miner. Resour. Res.* **2015**, *30*, 121–132.
40. Liu, X.D.; Zhou, T.F. General geological and geochemical characteristics and ore forming mechanism of the massive sulfide deposits. *J. Hefei Univ. Technol.* **1999**, *20*, 45–50.
41. Wang, Y.Q. Comparative Study on Sedex Deposits and VMS Deposits. *Resour. Environ. Eng.* **2009**, *23*, 259–262. [CrossRef]
42. Deng, Z.; Meng, G.X.; Qi, G.; Tang, H.J.; Xue, R.H.; Qing, J.H.; Wu, X.G.; Wang, X.J. Deep explanation model of the VMS-type deposit in the Ashele ore district. *Acta Geol. Sin.* **2025**, *99*, 1046–1060. [CrossRef]

Disclaimer/Publisher's Note: The statements, opinions and data contained in all publications are solely those of the individual author(s) and contributor(s) and not of MDPI and/or the editor(s). MDPI and/or the editor(s) disclaim responsibility for any injury to people or property resulting from any ideas, methods, instructions or products referred to in the content.